

Regio-selective Plasmonic Coupling in Metamolecular Analogs of Benzene Derivatives

Aiqin Fang,^{1, #} Sarah White,^{2, #} Prashant K. Jain,^{, 2} and Francis P. Zamborini^{*, 1}*

¹Department of Chemistry, University of Louisville, Louisville, KY 40292, USA

²Department of Chemistry, University of Illinois at Urbana-Champaign, Urbana, IL 61801, USA

*Corresponding authors E-mail: jain@illinois.edu, f.zamborini@louisville.edu

[#]equal contribution

SUPPORTING INFORMATION

EXPERIMENTAL DETAILS

Chemicals. Citric acid trisodium salt, L-ascorbic acid, sodium borohydride, cetyltrimethylammonium bromide (CTAB), mercaptopropyltrimethoxysilane (MPTMS), 1-hexanethiol (HT), 4-aminothiophenol (4-ATP), 2-propanol, ethyl alcohol, and acetone were purchased from Sigma-Aldrich. HAuCl₄·3H₂O was synthesized from metallic Au.

Synthesis of Au seeds and 25-nm diameter Au nanospheres (NSs). Small 3-5 nm diameter Au NSs, termed “Au seeds” were synthesized by adding 0.6 mL of ice cold 0.1 M NaBH₄ to 19 mL of an aqueous solution of 2.5 x 10⁻⁴ M trisodium citrate and 2.5 x 10⁻⁴ M HAuCl₄·3H₂O under stirring.¹ Two hours after the preparation of the Au seed solution, the seeds were used to synthesize

Au nanoplates (NPs), as described in the next section. ~25-nm diameter citrate-stabilized Au NSs were synthesized by adding 10 mL of a 1% sodium citrate solution to 100 mL of a boiling 2.5×10^{-4} M $\text{HAuCl}_4 \cdot 3\text{H}_2\text{O}$ solution. The mixed solution was kept stirring and boiling for 1 h and cooled down to room temperature with stirring before use. The ~25-nm diameter Au NS solutions were used 1 h after preparation.

Synthesis of Au NPs directly on glass surfaces with optimal size and coverage. Glass slides were prepared with etched number markings using photolithography, which was followed by a buffered oxide etch at the University of Louisville Micro/Nano Technology Center. Au nanostructures were synthesized directly on the glass slides using a seed-mediated growth method reported by our group recently,² but with a small modification designed to decrease the size and density of the NPs on the surface so that the sample would be amenable to single nanoparticle dark-field scattering studies. The glass slides were first functionalized with MPTMS by soaking in a solution of 10 mL of 2-propanol, 100 μL of MPTMS, and a few drops of water at a temperature of 95 °C for 30 min. After rinsing thoroughly with 2-propanol and drying under N_2 , the MPTMS-functionalized slides were then placed into a 1:10 diluted solution of Au seeds for 5 min, rinsed with Nanopure® water, and dried under N_2 . Next, the samples were placed into a Au growth solution containing 9.0 mL of 0.1 M cetyltrimethylammonium bromide (CTAB), 450 μL of 0.01 M $\text{HAuCl}_4 \cdot 3\text{H}_2\text{O}$, and 50 μL of 0.1 M ascorbic acid for 5 min, followed by rinsing with Nanopure® water, and drying under N_2 . In our previous work, we placed them in a growth solution for 1 h, which led to much larger Au NPs that are unsuitable for our single-nanoparticle scattering studies because of their broader, more red-shifted and complex scattering spectra. Following growth, the samples on the glass slides contain a mixture of Au NPs and Au NSs. The NSs and some NPs were removed by sonication for 10 min. This procedure led to samples with >90% Au NPs at a low

area-density, which is necessary for the single-nanoparticle dark-field scattering experiments. The NPs were determined by scanning electron microscopy (SEM) and atomic force microscopy (AFM) to be typically ~100 nm wide and ~30 nm thick.

Controlled attachment of Au NSs to the side faces/vertices of Au NPs. HT ligands were assembled onto the Au NPs and then place-exchanged with 4-ATP ligands. 4-ATP is a good bi-functional organic ligand that allows the coupling of citrate-coated Au NSs to Au NPs, since 4-ATP has a thiol group that attaches well to the Au NPs and an NH_2 group that, when protonated to NH_3^+ , allows electrostatic attachment of negatively-charged, citrate-coated Au NSs. The pH of the Au NS solution, which was maintained at 4.8 for all experiments, dictates the level of NH_2 protonation on 4-ATP and has a large impact on NS attachment.

In this procedure, we placed the glass slide with Au NPs in a 1 mM ethanolic solution of HT overnight. We rinsed the sample thoroughly with ethanol, followed by drying under N_2 , and then exchanged the HT monolayer with 4-ATP by placing the sample in a 6 mM ethanolic solution of 4-ATP for 1 h. We then rinsed the sample thoroughly with ethanol, followed by drying under N_2 . The substrates were then immersed in a 10-mL solution of ~25-nm diameter Au NSs for 30 min, rinsed thoroughly with Nanopure® water, and dried under N_2 . The thiol place-exchange occurs preferentially at side face/vertex sites of the NPs, which leads to a high density of 4-ATP at these sites and subsequently to preferential electrostatic binding of Au NSs at those sites.

Controlled attachment of Au NSs to terrace sites of Au NPs. In order to selectively bind the NSs to terrace sites, the samples were first placed in a 1 mM ethanolic solution of 4-ATP overnight, rinsed thoroughly with ethanol, and dried under N_2 . Then, we exchanged the 4-ATP with HT by placing the sample into a 6 mM ethanolic solution of HT for 4 h. We then rinsed the sample thoroughly with ethanol, following by drying under N_2 . Finally, the substrates were

immersed in 10 mL of a pH 4.8 solution of ~25-nm diameter Au NSs for 30 min, rinsed thoroughly with Nanopure® water, and dried under N₂. In this procedure, the original 4-ATP ligands on the Au NPs were displaced by HT preferentially at the side face/vertex sites, leading to the blocking of those regions from Au NS attachment and thereby to preferential binding of Au NSs to the terrace sites.

Spectroscopic and microscopic characterization. Scattering spectra were collected from individual NPs or coupled NP/NS assemblies using resonant Rayleigh dark-field scattering spectroscopy. Dark-field imaging was performed with an inverted Nikon Eclipse Ti microscope with a halogen lamp light source and a dark-field condenser (NA = 0.95-0.80) for sample illumination and a 100x variable aperture oil immersion objective (NA = 0.5-1.3) for collection of the scattered light from individual NPs or coupled NP/NS assemblies. An Infinity camera from Lumenera Corporation was used to obtain high-resolution video images for selecting individual scatterers. The detector used for measuring light scattering intensity as a function of wavelength was a multichannel air-cooled CCD camera used in a Horiba XPLORA-Inv confocal Raman system.

Scattering spectra obtained as a function of wavelength, were plotted in terms of energy units (eV) and then fit in OriginLab to single or multiple Lorentzian peaks, as noted. Peak maxima of scattering bands obtained in energy units (eV) were converted to wavelength units (nm). Coupling-induced LSPR shifts ($\Delta\lambda_{\text{max}}$) were determined from wavelength maxima.

DDA simulations of Au NPs and coupled NP/NS assemblies. The discrete dipole approximation (DDA) method was used for the simulation of LSPR spectra of Au NPs and for studying plasmon coupling of Au NPs with Au NSs. The DDA method numerically solves Maxwell's equations for one or a series of arbitrarily shaped objects by discretizing each object

into a cubic array of N polarizable point dipoles and self consistently solving for the polarizability of each dipole interacting with the incident field and all other $N-1$ dipoles. We employed the open source DDSCAT 7.3.0 code from Draine and Flatau.

The hexagonal NP target was generated via tools available on nanoHUB.org. A triangular mesh description of the hexagonal geometry was generated using the open-source 3D design tool “Blender”. Using the “DDSCAT Convert” tool (doi: 10.4231/D3FB4WM99), the geometry was discretized into a three-dimensional virtual dipole array, the input for DDSCAT. To simulate the dielectric properties of the ligand shell of NPs with Au NSs attached at the side faces/vertices, a 1-nm thick layer of HT ($n = 1.448$)³ was added to the surfaces of the top and bottom NP terraces and a 1-nm thick layer of 4-ATP ($n = 1.663$)⁴ was added to the surfaces of the side faces. Coupling between hexagonal NPs and NSs was simulated by attaching NSs to various sites on the side faces/vertices of the NP. To simulate the dielectric properties of the ligand shell of NPs with Au NSs attached at the terraces, a 1-nm thick layer of HT ($n = 1.448$)³ was added to the surfaces of the side faces and a 1-nm thick layer of 4-ATP ($n = 1.663$)⁴ was added to the surfaces of the top and bottom terraces. Au NSs of 27-nm diameter were generated using the DDSCAT subroutine CALLTARGET and combined with the NP target. For every case, the surface-to-surface separation distance between the NP and the NS was 1 nm, i.e., the NS was in contact with the ligand shell, which is the likely scenario in experiments. Note that this interparticle distance is measured along the thickness direction for NSs placed on the terraces and along one of the hexagonal axes for NSs placed on the side faces/vertices.

In order to match experimental conditions of dark-field scattering spectroscopy, all target structures were excited with unpolarized light, simulated by a circularly polarized plane wave, unless otherwise noted. Light, incident normal to the face of the NP, propagated along the thickness

of the NP. In all simulations, the refractive index of the ambient medium was set at $n_m = 1.1$, representative of a mixture of air ($n \approx 1$) and glass ($n \approx 1.5$). The relative contribution of air and glass was determined by the relative volume fraction of each within the surrounding medium, the surrounding medium being defined as the additional volume when the NP dimensions were extended 50% from the center of the NP along each axis. The bulk experimental dielectric function of Au from Johnson and Christy was utilized for all calculations without any corrections.

Scattering spectra (scattering efficiency vs. wavelength) were obtained from each simulation. Spectra were plotted in energy units (eV) and then fit in OriginLab to single or multiple Lorentzian peaks, as noted. Peak maxima of scattering bands obtained in energy units (eV) were converted to wavelength units (nm). Standard error was ca. 1 nm for all Lorentzian fits. Coupling-induced LSPR shifts ($\Delta\lambda_{\text{max}}$) were determined from wavelength maxima.

In addition to spectra, for four of the targets (a single NP, a NP coupled with a single NS on its terrace at two different interparticle distances, and a NP coupled with four NSs), near-field calculations were performed for specific light excitation conditions, i.e., wavelength and polarization. These near-field calculations utilized the DDSCAT 7.3 subroutine NEARFIELD. The macroscopic field amplitude $|E|$ at each grid-point of a volume surrounding the target structure was obtained relative to the incident field amplitude $|E_0|$, with the latter set to a value of 1. Near-field enhancements ($|E|/|E_0|$) were plotted over the surface of the target, using the open source application ParaView.

Table S1. LSPRs and SEM images of representative single Au NPs with a NS attached on the terrace.

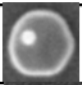

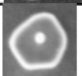
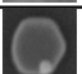
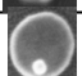
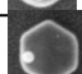
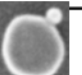
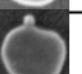
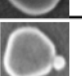
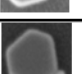
Initial λ_{\max} (nm)	Initial Peak Width (nm)	Final λ_{\max} (nm)	Final Peak Width (nm)	Shift (nm)	NS Size (nm)	Morphology
657	79	659	82	2	25	
659	112	661	104	2	26	
660	134	664	124	4	24	
679	103	682	105	3	23	
686	116	688	123	2	29	
707	120	709	117	2	25	
				Average =3±1	Average = 25±2	

Table S2. LSPRs and SEM images of representative single Au NPs with a NS attached on a side face/vertex

Initial λ_{\max} (nm)	Initial Peak Width (nm)	Final λ_{\max} (nm)	Final Peak Width (nm)	Shift (nm)	NS Size (nm)	Morphology
653	89	667	133	14	22	
673	82	696	88	23	20	
673	96	702	120	29	28	
678	94	699	138	21	27	
				Average =22±6	Average = 24±4	

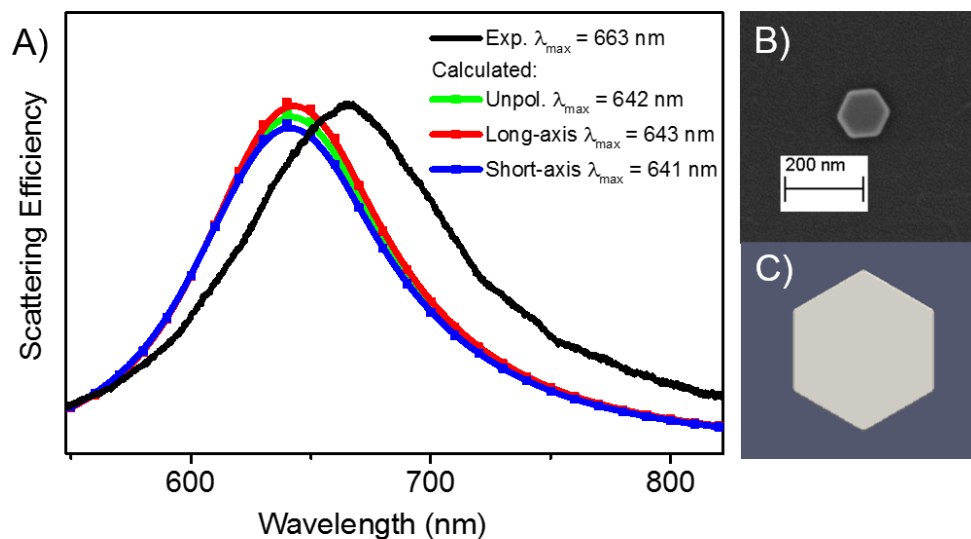


Figure S1. (A) Light-scattering spectrum of a single Au NP obtained via dark-field spectroscopy (black curve) and DDA simulations (red, green, and blue data-points). Wavelength maxima listed were determined by fitting spectra to single Lorentzian peaks. In one of the simulations, unpolarized light (green data-points connected by a cubic spline shown by the solid green curve) was employed for excitation, similar to the experimental conditions. Simulated spectra are also shown for incident light linearly polarized along the long in-plane axis of the NP (red data-points connected by a cubic spline shown by the solid red curve) and light polarized along the short in-plane axis of the NP (blue data-points connected by a cubic spline shown by the solid blue curve). Scattering spectra are similar for different polarization conditions, indicative of the small in-plane anisotropy of the hexagonal shape. (B) SEM image of the experimental nanoplate with a long-axis length of 136 nm and a thickness of 33 nm. (C) Rendition of the simulated structure, a Au NP with a long-axis length of 137 nm and a thickness of 31 nm, dimensions chosen to be closely representative of those obtained from SEM images for several experimental NPs. In summary, simulated spectra show good agreement with the experimental ones. Small differences are possibly due to small differences between i) the actual medium refractive index and the value used in the simulations and ii) the dimensions and/or edge curvature of the actual NPs and those idealized in the simulation.

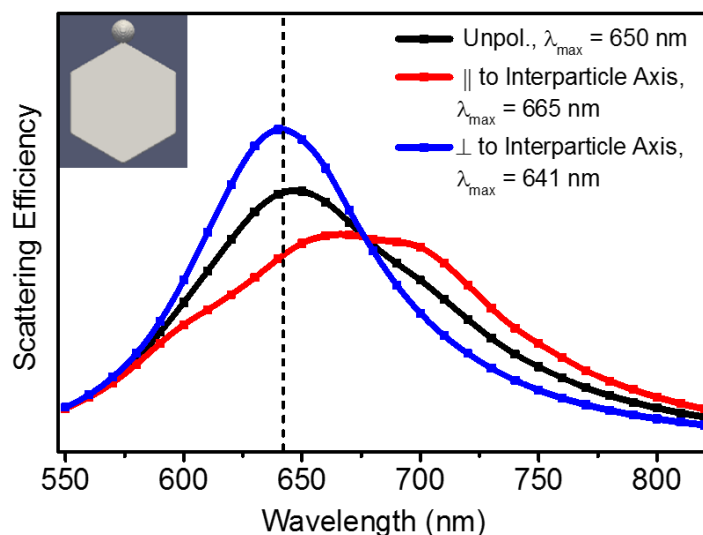


Figure S2. Simulated effect of incident light polarization on the plasmon coupling between a Au NP and a Au NS attached to a vertex on the side of the NP. Simulations were performed for a hexagonal Au NP with a long-axis length of 137 nm, a thickness of 31 nm, and a 1-nm thick ligand shell of HT and 4-ATP, representative of the experimental structure. A single Au NS, with a diameter of 27 nm, was attached to a vertex on the side of the NP, in the plane of the hexagon, as shown by the rendition in the inset. The distance between the surfaces of the NP and the NS was 1 nm, measured along the long axis of the hexagon. Wavelength maxima of scattering spectra were determined by fitting to single Lorentzian peaks. The dashed black line shows the λ_{max} for a NP without an attached NS. Relative to the peak position of this uncoupled case, coupling with the NS gives rise to a red-shift of 23 nm when the excitation light is polarized along the interparticle axis (red data-points connected by a cubic spline). On the other hand, there is a blue shift of 1 nm when light is polarized perpendicular to the interparticle axis (blue data-points connected by a cubic spline). This difference is consistent with the excitonic model of LSPR coupling.⁵ In the former case, the dipolar plasmon oscillations of the NP and NS are aligned head-to-tail, resulting in favorable coupling. In the latter case, the dipolar plasmon oscillations of the NP and NS are parallel to one another and therefore coupling between them is weakly repulsive. With unpolarized light excitation (black data-points connected by a cubic spline), the net strength of coupling and the extent of LSPR red-shift is intermediate between the two polarization extremes.

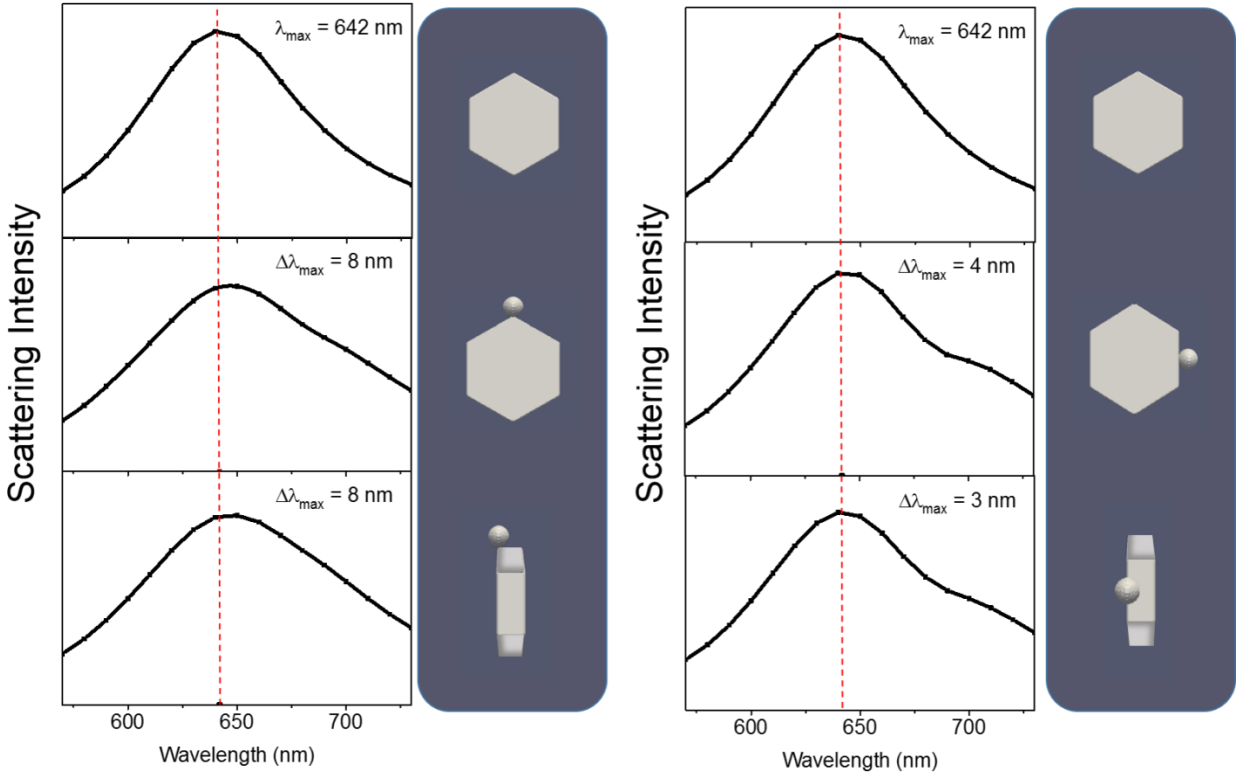


Figure S3. Simulated plasmon coupling between a Au NP and a Au NS: effect of the attachment location of the NS along the sides of the NP. Simulations were performed for a hexagonal Au NP with a long-axis length of 137 nm, a thickness of 31 nm, and a 1-nm thick ligand shell of HT and 4-ATP, representative of the experimental structure (top row). A single Au NS, 27 nm in diameter, was then placed at one of four select locations along the sides of the NP: at a vertex in the plane of the hexagon (left column, middle row), at the center of a side face in the plane of the hexagon (right column, middle row), at a vertex out of the plane of the hexagon (left column, bottom row), and at the center of a side face out of the plane of the hexagon (right column, bottom row). Renditions of these simulated configurations are shown beside each spectrum. The surfaces of the NS and the NP were separated by a distance of 1 nm, measured along one of the axes of the hexagon. Excitation was performed with unpolarized light. Spectra are shown as data-points connected by cubic splines (solid black curves). Wavelength maxima of scattering spectra were determined by fitting to single Lorentzian peaks. The dashed red line shows the λ_{max} for a NP without an attached NS. Relative to the peak position for this uncoupled case, coupling with the NS gives rise to a red-shift, indicated by $\Delta\lambda_{\text{max}}$. Of the cases considered, coupling is strongest when the NS is located at the vertex ($\Delta\lambda_{\text{max}} = 8$ nm), regardless of whether it is in the plane or out of the plane. Coupling is weaker for the cases where the NS is located at the center of a side face, away from the vertices. Also, for the cases where the NS is located on the side face of the NP, a noticeable shoulder emerges in the scattering spectrum; this feature affects somewhat the apparent red-shift obtained from the fit to a single Lorentzian peak. The coupling is slightly weaker for the out-of-plane side face location ($\Delta\lambda_{\text{max}} = 3$ nm) as compared to the in-plane side face location ($\Delta\lambda_{\text{max}} = 4$ nm).

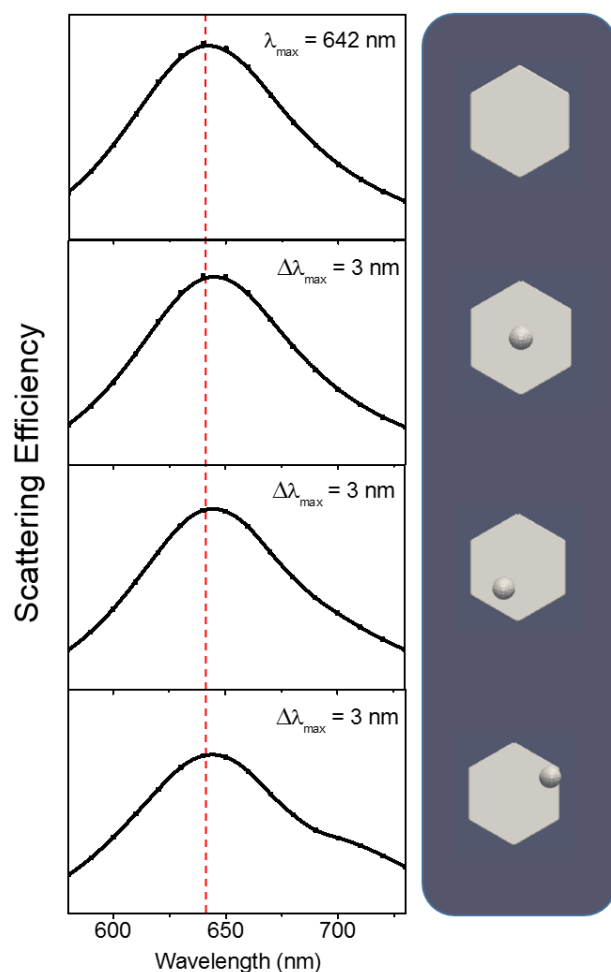


Figure S4. Simulated plasmon coupling between a hexagonal Au NP and a Au NS: effect of the location of the NS on the terrace of the NP. Simulations were performed for a hexagonal Au NP with a long-axis length of 137 nm, a thickness of 31 nm, and a 1-nm thick ligand shell of HT and 4-ATP, representative of the experimental structure (top row). A single Au NS, 27 nm in diameter, was then placed at one of three select locations on the terrace of the NP: at the center of the terrace (second row), close to the edge of the terrace (bottom row), and midway between these two locations (third row). Renditions of these simulated configurations are shown beside each spectrum. The surfaces of the NS and the NP were separated by a distance of 1 nm, measured along the thickness of the NP. Excitation was performed with unpolarized light. Spectra are shown as data-points connected by cubic splines (solid curves). Wavelength maxima of scattering spectra were determined by fitting to a single Lorentzian function. The dashed red line shows the λ_{max} for a NP without an attached NS. Relative to the peak position of this uncoupled case, coupling with the NS gives rise to a red-shift, indicated by $\Delta\lambda_{\text{max}}$. For all three positions, the $\Delta\lambda_{\text{max}}$ is 3 nm. Figure S6 shows that a terrace NS couples to the surface of the NP, but not necessarily to the NP dipolar mode, making the lateral position of the NS in relation to the NP edges less important. For the case where the NS is located at the edge of the terrace (bottom row), a noticeable shoulder emerges in the scattering spectrum; this feature affects somewhat the apparent red-shift obtained from the fit to a single Lorentzian peak.

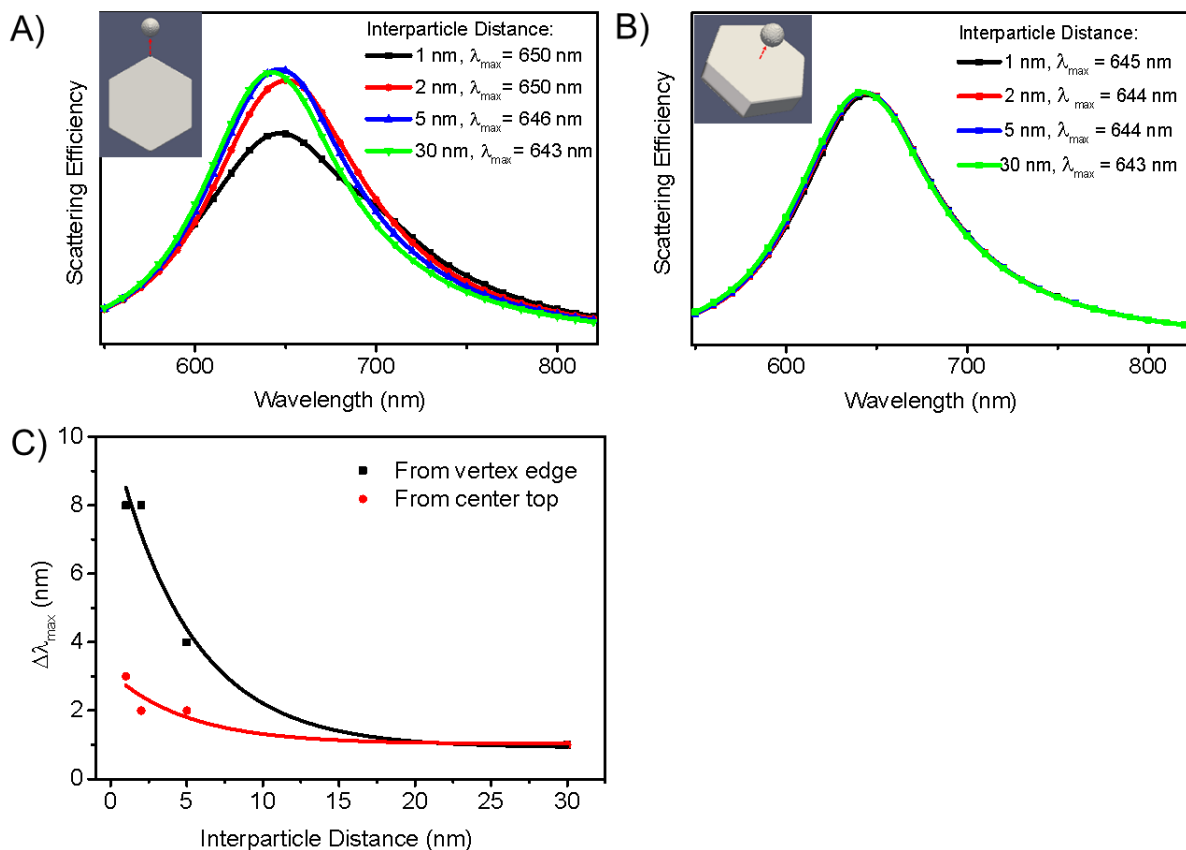


Figure S5. Simulated distance-dependence of plasmon coupling between a Au NP and a single Au NS for two cases: a NS placed at a vertex on the side (A) and a NS placed at the center of the terrace (B) as shown by the renditions in the insets. Simulations were performed for a hexagonal Au NP with a long-axis length of 137 nm, a thickness of 31 nm, and a 1-nm thick ligand shell of HT and 4-ATP, representative of the experimental structure. A single Au NS, 27 nm in diameter, was then placed either at the vertex on the side in the plane of the hexagon (A) or at the center of the terrace (B) at varying surface-to-surface interparticle distances. This distance was measured along the NP long axis for (A) and along the thickness direction for (B). Excitation was performed with unpolarized light. Spectra are shown as data-points connected by cubic splines (solid curves). Wavelength maxima of scattering spectra were determined by fitting to single Lorentzian peaks. The coupling-induced red-shift $\Delta\lambda_{\text{max}}$, relative to the LSPR peak position of a NP without an attached NS, is plotted in (C) as a function of surface-to-surface interparticle distance. The coupling strength, as indicated by the magnitude of the red-shift, increases with decreasing interparticle distance.

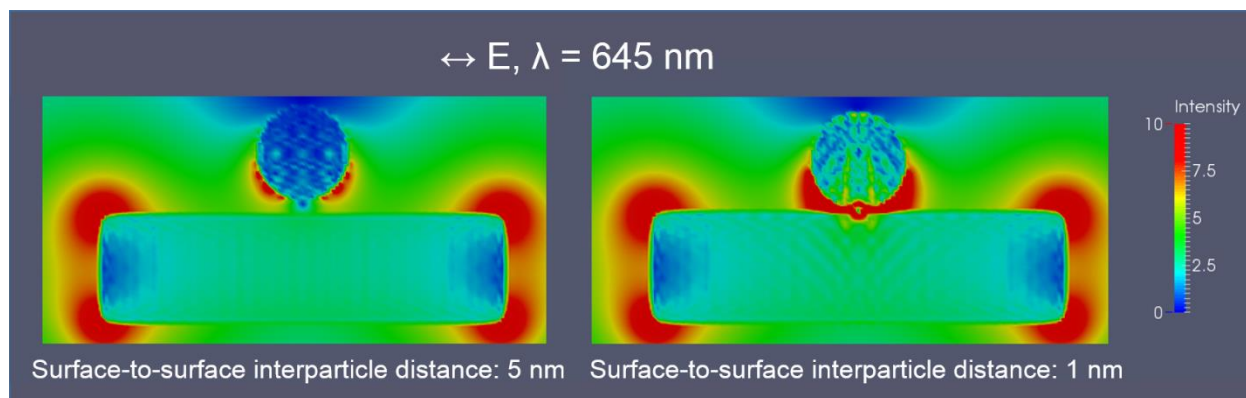


Figure S6. Simulated near-field of a Au NP coupled to a Au NS placed on the terrace of the NP. The images represent a side-view of a cross-section taken along the polarization direction. The near-field is depicted in the form of an amplitude enhancement ($|E|/|E_0|$) on a color scale. Simulations were performed for a hexagonal Au NP with a long-axis length of 137 nm, a thickness of 31 nm, and a 1-nm thick ligand shell of HT and 4-ATP, representative of the experimental structure, and a 27 nm diameter Au NS. For the left image, the surface-to-surface interparticle distance is 5 nm and for that on the right, it is 1 nm. Corresponding spectra are shown in Figure S5. The near-field pattern shows a strong dipolar mode excited in the NP. The NS placed 5 nm away from the NP exhibits an asymmetric near-field distribution: the near-field is concentrated on the NS surface that is closer to the NP. At a distance of 1-nm, the near-field is concentrated in the gap between the NS and NP, which is indicative of an attractive interaction between the dipolar plasmon oscillation of the NS and image dipoles induced on the surface of the NP.

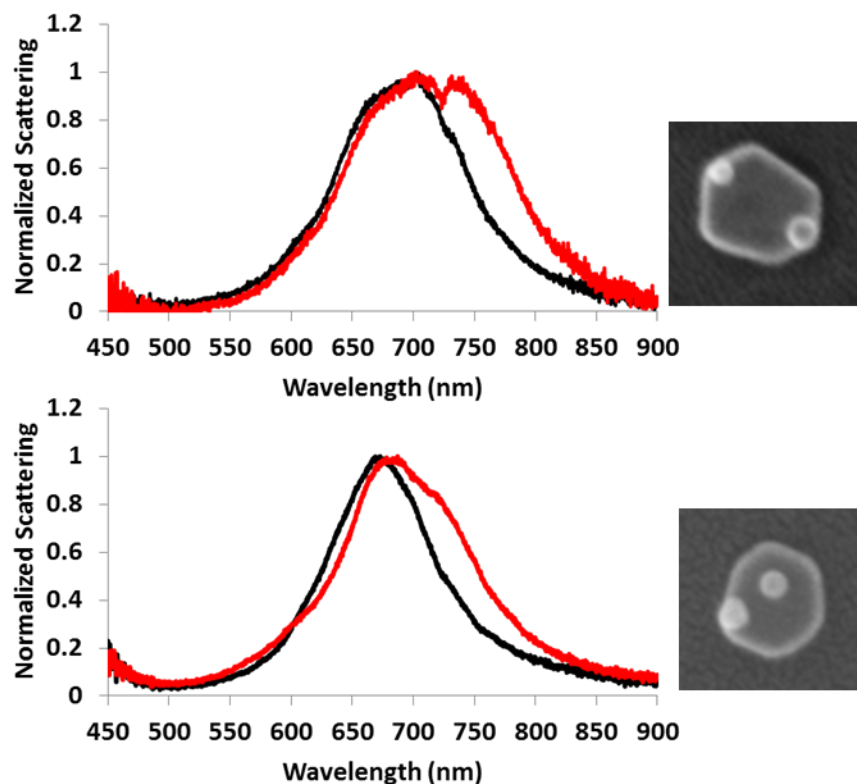


Figure S7. Single-particle dark-field light-scattering spectra of a Au NP before (black) and after (red) attachment of multiple NSs to NP terrace sites. Final morphologies are displayed on the right. When multiple NSs were distributed over inner terrace sites and near terrace edges, we often observed broadening resulting from the appearance of a new peak red-shifted as much as 35-40 nm relative to the dipolar mode of the uncoupled NP. This phenomenon is a result of increased symmetry breaking in the coupled NP/NS assemblies. This effect appeared to be starker when the initial NP itself was not very symmetric, as seen from the representative cases shown in this figure.

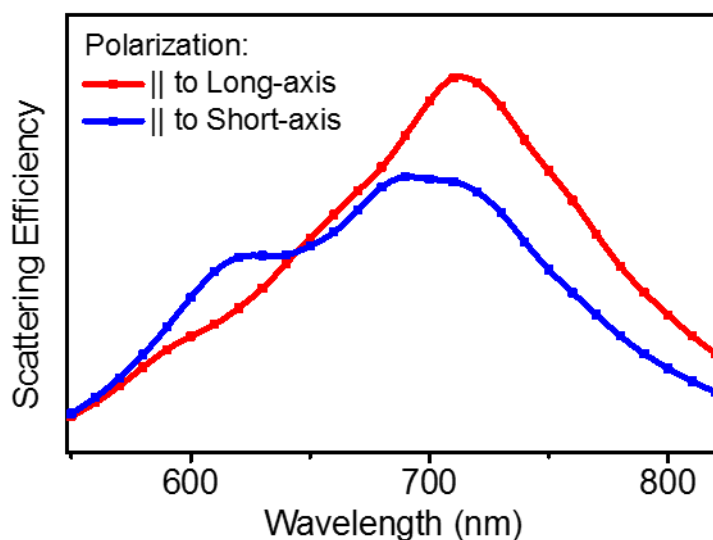


Figure S8. Simulated effect of the incident light polarization on the plasmon coupling between an Au NP and four NSs. Simulations were performed for a hexagonal Au NP with a long-axis length of 137 nm, a thickness of 31 nm, and a 1-nm thick ligand shell of HT and ATP, representative of the experimental structure. Four Au NSs, each with a diameter of 27 nm, were attached to four of the vertices of the NP, (configuration is shown in Figure S9). The surface-to-surface distance between the NP and each NS was 1 nm, measured along the long axis of the hexagon. The redshift in the dipolar LSPR resulting from coupling is smaller when light is polarized parallel to the short axis of the hexagon (blue data-points connected by a cubic spline) as compared to the case when light is polarized parallel to the long axis of the hexagon (red data-points connected by a cubic spline). However, under short-axis polarization, coupling results in the emergence of a prominent high energy mode centered at 613 nm, in addition to the dipolar mode at 705 nm. These λ_{max} values were determined by fitting the spectrum to two Lorentzian peaks. The scattering spectrum for long-axis polarization, fit to two Lorentzian peaks, yields a strong dipolar mode with a λ_{max} at 717 nm and only a weak shoulder in the blue region.

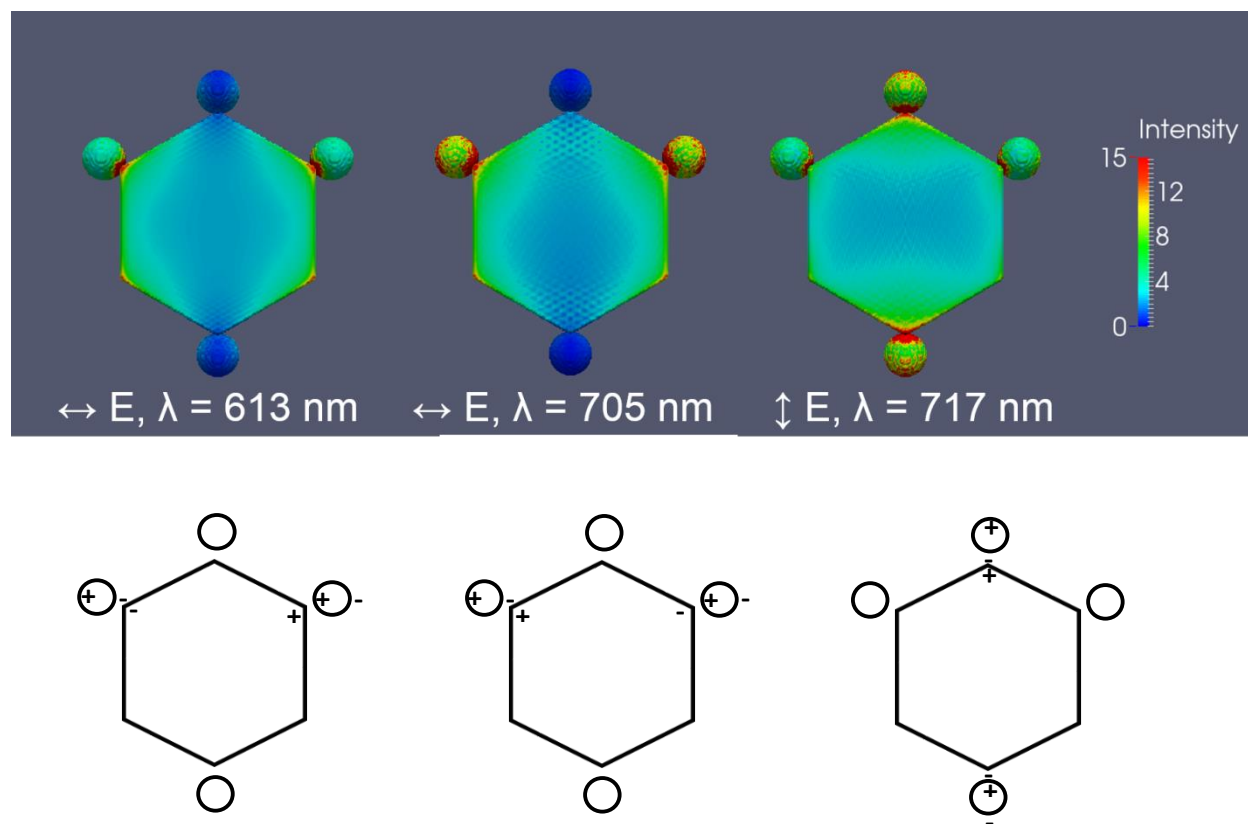


Figure S9. Simulated near-field over the surface of a Au NP coupled to four Au NSs. The near-field is depicted in the form of an amplitude enhancement ($|E|/|E_0|$) on a color scale. Simulations were performed for a hexagonal Au NP with a long-axis length of 137 nm, a thickness of 31 nm, and a 1-nm thick ligand shell of HT and 4-ATP, representative of the experimental structure. Four Au NSs, each with a diameter of 27 nm, were attached to four of the vertices of the NP, as depicted. The surface-to-surface distance between the NP and each NS was 1 nm, measured along the long axis of the hexagon. Three different simulations were run: the direction of polarization and wavelength of incident light employed in each simulation are noted for each near-field map. An electrostatic charge distribution corresponding to each near-field map is also shown below each map. When the incident light is polarized along the long axis of the hexagon (right panel), the near-field appears to be concentrated most at the extremities of the NSs located along the polarization direction, as well as at the junctions between the NS and NP vertices. As indicated by its respective electrostatic charge distribution, the field plot represents a dipolar mode of coupling between the NP and the two NSs, which is manifested as the LSPR peak centered at 717 nm in Figure S8. A similar dipolar mode of excitation is seen when light with a wavelength of 705 nm is polarized along the short axis of the hexagon (middle panel). However, when the short axis of the hexagon is excited using 613-nm wavelength light, corresponding to the higher energy peak in Figure S8, the field appears to be concentrated primarily at the junctions between the NS and NP vertex (left panel). There is lower field enhancement at the extremities of the NSs along the polarization direction. This field pattern is indicative of a higher-energy quadrupolar mode of excitation, as depicted by its respective electrostatic charge distribution.

Supporting Information References:

- ¹ Gole, A.; Murphy, C. J. *Chem. Mater.* **2004**, *16*, 3633-3640.
- ² Beeram, S. R.; Zamborini, F. P. *J. Am. Chem. Soc.* **2009**, *131*, 11689-11691.
- ³ Ochiai, T.; Isozaki, K.; Nishiyama, S.; Miki, K. *Appl. Phys. Exp.* **2014**, *7*, 65001.
- ⁴ Gabudean, A. M.; Biro, D.; Astilean, S. *J. Mol. Struct.* **2011**, *993*, 420-424.
- ⁵ Jain, P. K.; Eustis, S.; El-Sayed, M. A. *J. Phys. Chem. B* **2006**, *110*, 18243-18253.